Applied Mathematics and Computation 215 (2010) 3201–3213

Contents lists available at ScienceDirect

Applied Mathematics and Computation

journal homepage: www.elsevier.com/locate/amc

Upwind compact finite difference scheme for time-accurate solution of the incompressible Navier–Stokes equations

Abdullah Shah [a,b,*], Li Yuan [b], Aftab Khan [a]

[a] Department of Mathematics, COMSATS Institute of Information Technology, Islamabad, Pakistan
[b] LSEC, Institute of Computational Mathematics and Scientific/Engineering Computing, Academy of Mathematics and Systems Science, Chinese Academy of Sciences, Beijing 100190, PR China

ARTICLE INFO

Keywords:
Incompressible Navier–Stokes equation
Artificial compressibility method
Upwind compact finite difference
Flux-difference splitting
Dual-time stepping
Kovasznay flow problem
Oscillating plate
Taylor's decaying vortices
Doubly periodic shear layer

ABSTRACT

This article presents a time-accurate numerical method using high-order accurate compact finite difference scheme for the incompressible Navier–Stokes equations. The method relies on the artificial compressibility formulation, which endows the governing equations a hyperbolic–parabolic nature. The convective terms are discretized with a third-order upwind compact scheme based on flux-difference splitting, and the viscous terms are approximated with a fourth-order central compact scheme. Dual-time stepping is implemented for time-accurate calculation in conjunction with Beam-Warming approximate factorization scheme. The present compact scheme is compared with an established non-compact scheme via analysis in a model equation and numerical tests in four benchmark flow problems. Comparisons demonstrate that the present third-order upwind compact scheme is more accurate than the non-compact scheme while having the same computational cost as the latter.

1. Introduction

The viscous incompressible Navier–Stokes equations (INSE) are fundamental governing equations in fluid mechanics. The numerical solution of these equations is an indispensable tool for studying incompressible fluid flow problems. Numerous computational methods for solving these equations have been developed in the past five decades, see Refs. [1,2] for a review. However, with ever increasing interest in numerical calculations demanding high accuracy for a wide range of length scales, such as large-eddy simulation and direct numerical simulation of turbulence, high-order numerical methods become a major concern. Particularly, high-order finite difference, finite volume and finite element methods have received more attention than traditional globally high-order methods such as spectral methods [3,4] because the former are more robust in handling complicated geometries and boundary conditions than the latter.

High-order compact finite difference schemes [5–7] provide an effective way of combining the robustness of finite difference schemes and the accuracy of spectral methods. Generally, the computation of derivatives in compact finite differences is implicit in the sense that the derivative values at a particular node are computed not only from the function values but also from the values of the derivative at the neighboring nodes. The compact schemes are global schemes yet the computational cost is not high since solution of the resulting multi-diagonal sparse system can be carried out efficiently. Compared to non-compact schemes of the same order of accuracy, compact schemes utilize a smaller stencil, have smaller truncating errors,

* Corresponding author. Address: LSEC, Institute of Computational Mathematics and Scientific/Engineering Computing, Academy of Mathematics and Systems Science, Chinese Academy of Sciences, Beijing 100190, PR China.
E-mail addresses: abdullah@lsec.cc.ac.cn (A. Shah), lyuan@lsec.cc.ac.cn (L. Yuan).

0096-3003/$ - see front matter © 2009 Elsevier Inc. All rights reserved.
doi:10.1016/j.amc.2009.10.001

and give better resolution especially at higher wave numbers. Extensive study of high-order compact schemes on a uniform grid was carried out by Lele [7] in 1992. Since then compact schemes have attained wide popularity in solving various engineering problems involving incompressible [8,9,15,10–12] and compressible flows [13,14,16–19].

Compact finite difference schemes can generally be classified into two broad categories: central and upwind. Central compact schemes have the advantage of achieving higher-order accuracy with fewer grid points in the stencil, but they are non-dissipative, and using central compact schemes on non-staggered meshes for convection terms might cause numerical oscillations even for flows without discontinuities. Reducing or removing such oscillations requires the introduction of dissipation terms or the use of filtering approach [20]. However, filtering adds dissipation to the numerical scheme and this often results in a loss of sharp flow features in the computed solution [21], Furthermore, filtering is often treated implicitly and this again needs to solve multi-diagonal sparse system so as to double the computational cost for evaluating derivatives. In contrast, upwind compact schemes with dissipative properties do not need filtering. Fu and Ma [15,16] among others [17,22] have developed some upwind compact schemes. As these upwind compact schemes can automatically provide grid-scale linkage for each variable to avoid odd-even decoupling and built-in dissipation mechanism to prevent non-physical oscillations, they are suitable for discretizing the convective terms on collocated grids for the primitive formulation, and this will make it easy to develop solution methods capable of handling problem with complicated geometries.

The difficulty in solving the primitive variable form of the INSE is the lack of a time derivative term in the continuity equation, which limits the straight forward application of time marching numerical methods. Some of the primitive variable formulations for solving these equations are MAC method [23], fractional step (or projection) methods [24,25], SIMPLE method [26], and the artificial compressibility (AC) method [27]. It is remarked that designing a higher than three-order projection method or SIMPLE method is a nontrivial task. However, it is quite straight forward to develop high-order schemes based on the AC method.

The AC method has been extensively developed for time-accurate flow computation by many investigators including [28–32]. The common way is to add pseudo-time derivatives to the continuity equation as well as the momentum equations, and then to utilize dual-time stepping technique [30,31], i.e., in each physical-time step, sub-iteration are performed to drive the velocity divergence to zero. Various discretization and solution strategies borrowed from compressible flow methods were implemented in conjunction with the AC method, such as upwind biased schemes based on flux-difference splitting (FDS) [28,29,33], MUSCL scheme [34,32] and WENO scheme [35]. However, applications of compact schemes in conjunction with the AC method are quite few [36,37].

The objective of the present study is to extend our previous work [37] for steady state problems to time-accurate simulation of unsteady incompressible flow problems. The upwind compact scheme developed in [37] combined Fu and Ma's upwind compact scheme [15,16] with flux-difference splitting. The advantage of Fu and Ma's upwind compact schemes lies in that, their implicit parts involve only two points while most other upwind compact schemes involve three or five points [18,38]. This will reduce a reasonable amount of computational costs.

In this paper, implementation of the flux-difference splitting based third-order upwind compact scheme [37] for the convective terms in Cartesian coordinates is given in detail. The explicit part of the compact scheme is computed according to Rogers' implementation of flux-difference splitting [28], while the implicit part of the compact scheme retains the same bi-diagonal equations as Fu and Ma's upwind compact scheme [15,16]. To show the third-order accuracy for our upwind compact scheme, we employ a fourth-order central compact scheme for the viscous terms. We use the well established dual time stepping technique [30,31] for achieving time accuracy. The efficiency of the sub-iteration procedure is not concerned in this paper, so the traditional Beam-Warming approximate factorization scheme is used. The accuracy and efficiency of the present upwind compact schemes are compared with the established non-compact scheme [28,29] through numerical tests in several two-dimensional benchmark problems.

The rest of the paper is organized as follows: In Section 2, formulations for the artificial compressibility method are briefly outlined. Section 3 describes the spatial discretization including the upwind compact scheme and the non-compact scheme for the convective terms. Section 4 describes the solution method to the discretized equations. In Section 5 boundary conditions are given. Section 6 deals with analysis of the compact and non-compact schemes in a model problem. Tests for order of accuracy and comparison with the non-compact scheme are made via calculating several 2D unsteady flow problems in Section 7. Finally, conclusions are drawn in Section 8.

2. Governing equations

The governing equations for two-dimensional incompressible Navier–Stokes equations in Cartesian coordinates (x, y) in dimensionless form and in the absence of body forces are:

$$\nabla \cdot \mathbf{u} = 0, \tag{2.1}$$

$$\mathbf{u}_t + (\mathbf{u} \cdot \nabla)\mathbf{u} + \nabla p - \frac{1}{\mathrm{Re}}\nabla^2 \mathbf{u} = 0, \tag{2.2}$$

here $\mathbf{u}$ is the velocity field, p is the static pressure and Re is the Reynolds number. By introducing pseudo-time terms into the continuity and momentum equations with the dual-time stepping technique (pseudo-time τ + physical-time t), we have [28]:

$$\frac{\partial p}{\partial \tau}+\beta\left(\frac{\partial u}{\partial x}+\frac{\partial v}{\partial y}\right)=0, \tag{2.3}$$

$$\frac{\partial u}{\partial \tau}+\frac{\partial u}{\partial t}+\frac{\partial (u^2+p)}{\partial x}+\frac{\partial (uv)}{\partial y}-\frac{1}{\mathrm{Re}}\left(\frac{\partial u_x}{\partial x}+\frac{\partial u_y}{\partial y}\right)=0, \tag{2.4}$$

$$\frac{\partial v}{\partial \tau}+\frac{\partial v}{\partial t}+\frac{\partial (uv)}{\partial x}+\frac{\partial (v^2+p)}{\partial y}-\frac{1}{\mathrm{Re}}\left(\frac{\partial v_x}{\partial x}+\frac{\partial v_y}{\partial y}\right)=0, \tag{2.5}$$

where β is the artificial compressibility parameter whose value is important to the performance of the AC method. Eqs. 2.3, 2.4 and 2.5 can also be written as

$$\frac{\partial \mathbf{Q}}{\partial \tau}+\mathbf{I}_m\frac{\partial \mathbf{Q}}{\partial t}+\frac{\partial (\mathbf{E}-\mathbf{E}_v)}{\partial x}+\frac{\partial (\mathbf{F}-\mathbf{F}_v)}{\partial y}=\mathbf{0}. \tag{2.6}$$

where $\mathbf{Q}=[p,u,v]^T$ is the solution variable vector, $\mathbf{E}$, $\mathbf{F}$, and $\mathbf{E}_v,\mathbf{F}_v$ are the inviscid and viscous flux vectors, respectively i.e.,

$$\mathbf{E}=\begin{bmatrix}\beta u\\ u^2+p\\ uv\end{bmatrix},\quad \mathbf{F}=\begin{bmatrix}\beta v\\ uv\\ v^2+p\end{bmatrix},\quad \mathbf{E}_v=\frac{1}{\mathrm{Re}}\begin{bmatrix}0\\ u_x\\ v_x\end{bmatrix},\quad \mathbf{F}_v=\frac{1}{\mathrm{Re}}\begin{bmatrix}0\\ u_y\\ v_y\end{bmatrix}.$$

The matrix $\mathbf{I}_m=\mathrm{diag}(0,1,1)$ is a modified identity matrix.

Because of the added AC term, the equations become hyperbolic type in time, with flux Jacobian matrices $\mathbf{A}$ and $\mathbf{B}$ being

$$\mathbf{A}=\frac{\partial \mathbf{E}}{\partial \mathbf{Q}}=\begin{bmatrix}0&\beta&0\\1&2u&0\\0&v&u\end{bmatrix},\quad \mathbf{B}=\frac{\partial \mathbf{F}}{\partial \mathbf{Q}}=\begin{bmatrix}0&0&\beta\\0&v&u\\1&0&2v\end{bmatrix}.$$

It is possible to diagonalize $\mathbf{A}$ and $\mathbf{B}$ by using similarity transform as

$$\mathbf{A}=\mathbf{X}\boldsymbol{\Lambda}_A\mathbf{X}^{-1},\quad \mathbf{B}=\mathbf{Y}\boldsymbol{\Lambda}_B\mathbf{Y}^{-1},$$

where diagonal matrices $\boldsymbol{\Lambda}_A$ and $\boldsymbol{\Lambda}_B$ contain the eigenvalues of matrices $\mathbf{A}$ and $\mathbf{B}$:

$$\mathrm{diag}(\boldsymbol{\Lambda}_A)=\{u-c_1,u,u+c_1\},\mathrm{diag}(\boldsymbol{\Lambda}_B)=\{v-c_2,v,v+c_2\},$$

with $c_1=\sqrt{u^2+\beta}$ and $c_2=\sqrt{v^2+\beta}$ being the pseudo-speeds of sound in both directions. $\mathbf{X}$ and $\mathbf{Y}$ are the matrices of the right eigenvectors, while $\mathbf{X}^{-1}$ and $\mathbf{Y}^{-1}$ are their inverses, respectively. The eigenvalues of the Jacobian matrix play an important role in understanding the mathematical characteristics of the governing equations. More importantly, it gives us the speed and direction of propagation of information providing basis for the development of an upwind scheme.

3. Spatial discretization

3.1. Third-order upwind compact scheme

Due to the hyperbolic nature of the system (2.6), the convective terms can be split in two parts, i.e., along the x-direction

$$\mathbf{E}_x=\mathbf{E}_x^+ +\mathbf{E}_x^-. \tag{3.1}$$

$\mathbf{E}^+$ corresponds to the flux in the positive x direction with information being propagated from left to right by the positive eigenvalues and $\mathbf{E}^-$ corresponds to the flux in the negative x direction with information being propagated from right to left by the negative eigenvalues. To evaluate the split derivatives, we use the third-order upwind compact scheme developed by Fu and Ma [15,16] in the following form

$$\frac{2}{3}(\mathbf{E}_x^+)_i+\frac{1}{3}(\mathbf{E}_x^+)_{i-1}=\frac{5\bigtriangledown_i\mathbf{E}^+ +\bigtriangleup_i\mathbf{E}^+}{6\Delta x},\quad \mathcal{O}(\Delta x^3) \tag{3.2a}$$

$$\frac{2}{3}(\mathbf{E}_x^-)_i+\frac{1}{3}(\mathbf{E}_x^-)_{i+1}=\frac{\bigtriangledown_i\mathbf{E}^- +5\bigtriangleup_i\mathbf{E}^-}{6\Delta x},\quad \mathcal{O}(\Delta x^3) \tag{3.2b}$$

where $\bigtriangleup_i f=f_{i+1}-f_i$ and $\bigtriangledown_i f=f_i-f_{i-1}$. Eq. (3.2b) can be explicitly marched forward and Eq. (3.2a) backward to get all the derivatives once the right-hand side (RHS) and the boundary derivative is given. The RHS of (3.2b) and (3.2a) involves the difference of split fluxes between neighboring points, which can be computed with flux-difference splitting (FDS) originally being approximate Riemann solver for the Euler equations [39]. The Roe formula is [39]:

$$\mathbf{E}_{i+1}^{\pm}-\mathbf{E}_i^{\pm}\equiv\bigtriangleup\mathbf{E}_{i+\frac{1}{2}}^{\pm}=\mathbf{A}^{\pm}(\overline{\mathbf{Q}})(\mathbf{Q}_{i+1}-\mathbf{Q}_i), \tag{3.3}$$

where $\bigtriangleup\mathbf{E}_{i+\frac{1}{2}}^{\pm}$ is the flux difference across the positive or negative traveling waves. The split Jacobian matrix is calculated by $\mathbf{A}^{\pm}(\overline{\mathbf{Q}})=\mathbf{X}\boldsymbol{\Lambda}_A^{\pm}\mathbf{X}^{-1}$ with $\boldsymbol{\Lambda}_A^{\pm}=\frac{1}{2}(\boldsymbol{\Lambda}_A\pm|\boldsymbol{\Lambda}_A|)$, which is evaluated using some intermediate value $\overline{\mathbf{Q}}$. For incompressible flows, the

Roe properties [39], which are necessary for a conservative scheme, are satisfied if $\overline{\mathbf{Q}}$ is taken as the arithmetic average of the surrounding points [28,29,33]

$$\overline{\mathbf{Q}} = \frac{1}{2}(\mathbf{Q}_i + \mathbf{Q}_{i+1}).$$

To close the third-order interior scheme, an explicit, dissipative, and third-order one-sided boundary scheme [19] is used at boundary points:

$$\text{at } i = 1: \quad (\mathbf{E}_x^+)_i = \frac{-11\mathbf{E}_i^+ + 18\mathbf{E}_{i+1}^+ - 9\mathbf{E}_{i+2}^+ + 2\mathbf{E}_{i+3}^+}{6\Delta x} = \frac{11\Delta\mathbf{E}_{i+\frac{1}{2}}^+ - 7\Delta\mathbf{E}_{i+\frac{3}{2}}^+ + 2\Delta\mathbf{E}_{i+\frac{5}{2}}^+}{6\Delta x}, \quad \mathcal{O}(\Delta x^3), \tag{3.4a}$$

$$\text{at } i = N: \quad (\mathbf{E}_x^-)_i = \frac{11\mathbf{E}_i^- - 18\mathbf{E}_{i-1}^- + 9\mathbf{E}_{i-2}^- - 2\mathbf{E}_{i-3}^-}{6\Delta x} = \frac{11\Delta\mathbf{E}_{i-\frac{1}{2}}^- - 7\Delta\mathbf{E}_{i-\frac{3}{2}}^- + 2\Delta\mathbf{E}_{i-\frac{5}{2}}^-}{6\Delta x}, \quad \mathcal{O}(\Delta x^3). \tag{3.4b}$$

3.2. Third-order non-compact scheme

The established third-order upwind biased scheme in Refs. [28,29] essentially is

$$(\mathbf{E}_x^+)_i = \frac{2\Delta\mathbf{E}_{i+\frac{1}{2}}^+ + 5\Delta\mathbf{E}_{i-\frac{1}{2}}^+ - \Delta\mathbf{E}_{i-\frac{3}{2}}^+}{6\Delta x}, \quad \mathcal{O}(\Delta x^3), \tag{3.5a}$$

$$(\mathbf{E}_x^-)_i = \frac{2\Delta\mathbf{E}_{i-\frac{1}{2}}^- + 5\Delta\mathbf{E}_{i+\frac{1}{2}}^- - \Delta\mathbf{E}_{i+\frac{3}{2}}^-}{6\Delta x}, \quad \mathcal{O}(\Delta x^3). \tag{3.5b}$$

We compare computational counts between Eqs. (3.5b), (3.5a) and (3.2b), (3.2a) with given boundary derivatives. We find both the upwind compact scheme and the non-compact scheme have identical computational cost.

3.3. Fourth-order central compact scheme for the viscous terms

The discretization of the viscous terms is much more simpler than that of the convective terms because viscous diffusion occurs in all directions, and the discretization of the viscous terms is always performed with central formulas. Therefore, the second derivative in the viscous terms of Eq. (2.6) is approximated by a fourth-order central compact scheme [16], i.e.,

$$\frac{1}{12}(S_{i-1} + 10S_i + S_{i+1}) = \frac{u_{i-1} - 2u_i + u_{i+1}}{\Delta x^2}, \tag{3.6}$$

where S approximates $\partial^2 u/\partial x^2$ in fourth-order accuracy. To obtain S_i, a linear system of equations with a tri-diagonal matrix has to be solved.

4. AF Scheme

The approximate factorization (AF) method [40] is an extension of the alternating direction implicit (ADI) method to the system of the Navier–Stokes equations. Direct solution methods exist but are computationally expensive, thus the approximate factorization scheme is a better choice. By applying backward difference to the pseudo-time derivative and three point, second-order backward difference scheme to the physical-time derivative, one obtains

$$\frac{\Delta\mathbf{Q}^{n+1,m}}{\Delta\tau} + \mathbf{I}_m\frac{1.5\mathbf{Q}^{n+1,m+1} - 2\mathbf{Q}^n + 0.5\mathbf{Q}^{n-1}}{\Delta t} = -\left[\frac{\partial(\mathbf{E} - \mathbf{E}_v)}{\partial x} + \frac{\partial(\mathbf{F} - \mathbf{F}_v)}{\partial y}\right]^{n+1,m+1} = \mathbf{R}^{n+1,m+1} \tag{4.1}$$

where $\Delta\mathbf{Q}^{n+1,m} = \mathbf{Q}^{n+1,m+1} - \mathbf{Q}^{n+1,m}$, the superscript n is the physical-time level, and m is the pseudo-time level (the number of sub-iterations). $\Delta\tau$ is the pseudo-time step size which is determined based on the CFL number and Δt is the physical-time step size. For the unsteady formulation, the equations are iterated in pseudo-time so that $\mathbf{Q}^{n+1,m+1}$ approaches the physical $\mathbf{Q}^{n+1}$ as the iteration is converged. The residual terms at $m+1$ pseudo-time level are linearized with respect to the previous level m by using Taylor's expansion, e.g.,

$$\mathbf{E}^{m+1} \approx \mathbf{E}^m + \left(\frac{\partial\mathbf{E}}{\partial\mathbf{Q}}\right)^m(\mathbf{Q}^{m+1} - \mathbf{Q}^m) = \mathbf{E}^m + \mathbf{A}^m\Delta\mathbf{Q}^m. \tag{4.2}$$

From now on, the superscript $n+1$ is omitted for brevity. One can obtain the unfactored implicit delta form as

$$\left[\mathbf{I} + 1.5\frac{\Delta\tau}{\Delta t}\mathbf{I}_m + \Delta\tau\left(\frac{\partial(\mathbf{A} - \mathbf{A}_v)}{\partial x} + \frac{\partial(\mathbf{B} - \mathbf{B}_v)}{\partial y}\right)\right]^m\Delta\mathbf{Q}^m = -\Delta\tau\left(\frac{\partial(\mathbf{E} - \mathbf{E}_v)}{\partial x} + \frac{\partial(\mathbf{F} - \mathbf{F}_v)}{\partial y}\right)^m - \frac{\Delta\tau}{\Delta t}\mathbf{I}_m(1.5\mathbf{Q}^m - 2\mathbf{Q}^n + 0.5\mathbf{Q}^{n-1}) = \mathbf{S}^m, \tag{4.3}$$

where

$$\mathbf{S}^m = \Delta\tau\mathbf{R}^m - \frac{\Delta\tau}{\Delta t}\mathbf{I}_m(1.5\mathbf{Q}^m - 2\mathbf{Q}^n + 0.5\mathbf{Q}^{n-1}).$$

The terms $\mathbf{A}_v$ and $\mathbf{B}_v$ are the viscous Jacobian matrices. For the steady state formulation, terms resulting from derivatives with respect to t are dropped and the time level $n+1$ represents the steady state. The equations are marched in pseudo-time until RHS of Eq. (4.3) converges to zero. The Beam-Warming approximate factorization (AF) scheme [40] can be symbolically written as

$$\pounds \cdot \Delta\mathbf{Q}^m \approx \pounds_x \pounds_y \cdot \Delta\mathbf{Q}^m = \mathbf{S}^m. \tag{4.4}$$

To obtain block tri-diagonal equations, convective terms in LHS of Eq. (4.3) are discretized by first-order upwind difference and viscous terms by traditional central difference, e.g.,

$$\delta_x^+ f_i = \frac{f_{i+1} - f_i}{\Delta x}, \quad \delta_x^- f_i = \frac{f_i - f_{i-1}}{\Delta x}, \text{ and } \quad \delta_x^2 f_i = \frac{(f_{i+1} - 2f_i + f_{i-1})}{\Delta x^2}.$$

Remember that the upwind compact scheme is used only for the RHS. Thus, one obtains the following form

$$\left[\mathbf{I} + 1.5\frac{\Delta\tau}{\Delta t}\mathbf{I}_m + \Delta\tau\left(\delta_x^-\mathbf{A}^+ + \delta_x^+\mathbf{A}^- - \delta_x\mathbf{A}_v\right) + \Delta\tau\left(\delta_y^-\mathbf{B}^+ + \delta_y^+\mathbf{B}^- - \delta_y\mathbf{B}_v\right)\right]^m \Delta\mathbf{Q}^m = \mathbf{S}^m. \tag{4.5}$$

Let $\mathbf{I}_m \to \mathbf{I}$ to make diagonalization possible and denote $(1 + 1.5\frac{\Delta\tau}{\Delta t})\mathbf{I} = \mathbf{H}$, then

$$\left[\mathbf{H} + \Delta\tau\left(\delta_x^-\mathbf{X}\boldsymbol{\Lambda}_A^+\mathbf{X}^{-1} + \delta_x^+\mathbf{X}\boldsymbol{\Lambda}_A^-\mathbf{X}^{-1} - \frac{\mathbf{I}}{\mathrm{Re}}\delta_x^2\right) + \Delta\tau\left(\delta_y^-\mathbf{Y}\boldsymbol{\Lambda}_B^+\mathbf{Y}^{-1} + \delta_y^+\mathbf{Y}\boldsymbol{\Lambda}_B^-\mathbf{Y}^{-1} - \frac{\mathbf{I}}{\mathrm{Re}}\delta_y^2\right)\right]^m \Delta\mathbf{Q}^m = \mathbf{S}^m. \tag{4.6}$$

Finally, by adding cross-derivative terms only to the LHS, which is the same order of $\Delta\tau^3$ as the truncated terms of original equations, we can obtain the AF scheme in the following form

$$\left[\mathbf{H} + \Delta\tau\left(\delta_x^-\mathbf{X}\boldsymbol{\Lambda}_A^+\mathbf{X}^{-1} + \delta_x^+\mathbf{X}\boldsymbol{\Lambda}_A^-\mathbf{X}^{-1} - \frac{\mathbf{I}}{\mathrm{Re}}\delta_x^2\right)\right]\mathbf{H}^{-1} \times \left[\mathbf{H} + \Delta\tau\left(\delta_y^-\mathbf{Y}\boldsymbol{\Lambda}_B^+\mathbf{Y}^{-1} + \delta_y^+\mathbf{Y}\boldsymbol{\Lambda}_B^-\mathbf{Y}^{-1} - \frac{\mathbf{I}}{\mathrm{Re}}\delta_y^2\right)\right]\Delta\mathbf{Q}^m = \mathbf{S}^m \tag{4.7}$$

The system (4.7) can be solved with the well-known ADI scheme. To reduce computational cost further, we adopt the diagonalization procedure [41] to put the left and right eigenvector matrices out of the difference operators to obtain

$$\left[\mathbf{H} + \Delta\tau\left(\delta_x^-\boldsymbol{\Lambda}_A^+ + \delta_x^+\boldsymbol{\Lambda}_A^- - \frac{1}{\mathrm{Re}}\delta_x^2\right)\right]\Delta\mathbf{Q}^{**} = \mathbf{X}^{-1}\mathbf{S}^m, \tag{4.8a}$$

$$\left[\mathbf{H} + \Delta\tau\left(\delta_y^-\boldsymbol{\Lambda}_B^+ + \delta_y^+\boldsymbol{\Lambda}_B^- - \frac{1}{\mathrm{Re}}\delta_y^2\right)\right]\Delta\mathbf{Q}^{*} = \mathbf{Y}^{-1}\mathbf{H}\mathbf{X}\Delta Q^{**}, \tag{4.8b}$$

$$\Delta\mathbf{Q}^m = \mathbf{Y}\Delta\mathbf{Q}^{*}. \tag{4.8c}$$

Eq. (4.8c) or (4.8a) is a system of scalar tri-diagonal equations of the form

$$\alpha_i\Delta\mathscr{U}_{i-1} + \beta_i\Delta\mathscr{U}_i + \gamma_i\Delta\mathscr{U}_{i+1} = r_i, \quad i = 2, \ldots, \mathrm{imax} - 1$$

with Dirichlet boundary condition $\Delta\mathscr{U}_1 = \Delta\mathscr{U}_{\mathrm{imax}} = 0$ for general cases, and periodic boundary condition for periodic cases.

In order to provide enough damping for numerical stability, the split eigenvalues in LHS of Eqs. (4.8c) and (4.8a) are constructed as

$$\boldsymbol{\Lambda}^{\pm} = \frac{1}{2}(\boldsymbol{\Lambda} \pm \kappa|\boldsymbol{\Lambda}|),$$

where κ is a constant that is greater than or equal to unity to ensure the split eigenvalue is strictly positive or negative.

5. Boundary conditions

The boundary conditions at a wall are specified as follows. The velocity satisfies a Dirichlet condition. For a viscous flow, the boundary condition on the wall is non-penetration and non-slip, i.e., the velocity is equal to zero. If the problem includes a moving wall, then the given wall velocity is specified. The pressure at a wall boundary is obtained by setting the pressure gradient normal to the wall to be zero. Symmetric or periodic boundary conditions are imposed in the symmetry plane. The boundary conditions at the inflow and outflow boundaries can be defined by considering the characteristic waves traveling in and out of the computational domain. For each positive (or negative) eigenvalue, there is a wave propagating information in the positive (or negative) direction. Therefore, we can use the eigenvalues to determine the characteristic waves that bring information from the interior of the domain to the boundaries.

In the ADI procedure, all the boundary conditions are generally treated explicitly because of the lack of physical meaning for $\Delta\mathbf{Q}^*$ and $\Delta\mathbf{Q}^{**}$ at split steps, which can be achieved by setting them to zero on the boundary. However, for a problem with

periodic boundary conditions, the boundary is treated implicitly and a periodic scalar- or block-tridiagonal solver [42] is used to solve the system.

6. Model problem

In order to examine approximating behavior of the upwind compact scheme, we use the following model equation as suggested in Ref. [19] and its semi-discrete approximation as follows:

$$\frac{\partial u}{\partial t} + c\frac{\partial u}{\partial x} = 0, \quad c > 0, \tag{6.1a}$$

$$\frac{\partial u_j}{\partial t} + cF_j = 0, \tag{6.1b}$$

where F_j is the finite difference approximation to $\partial u/\partial x$. With the initial condition $u(x,0) = e^{ikx}$, the exact solution of Eq. (6.1a) is $u(x,t) = e^{ik(x-ct)}$, and the exact solution of Eq. (6.1b) can be written as $u(x_j,t) = e^{-k_i\frac{ct}{\Delta x}}e^{ik\left(x_j-\frac{k_r}{k\Delta x}ct\right)}$, where the modified wave number $k_e = k_r + ik_i$ can be obtained from a given difference scheme. k_r is related to the numerical damping of a difference scheme and k_i is related to the phase speed in the numerical solution. For the third-order upwind compact scheme Eq. (3.2a),

$$k_r = \frac{(1-\cos\alpha)^2}{5+4\cos\alpha}, \quad k_i = \frac{\sin\alpha(8+\cos\alpha)}{5+4\cos\alpha}, \tag{6.2}$$

where the reduced wave number is $\alpha = k\Delta x$. For the explicit third-order upwind scheme of Rogers and Ewak [29],

$$k_r = \frac{1}{6}(3-4\cos\alpha+\cos 2\alpha), \quad k_i = \frac{1}{6}(8\sin\alpha - \sin 2\alpha). \tag{6.3}$$

Fig. 1 shows variations of k_i and k_r with the reduced wave number α for the upwind compact scheme and the upwind biased scheme of Ref. [29]. We can see the compact scheme can approximate the exact dispersion relation ($k_i^E = \alpha$) better than the non-compact scheme. From the curve of k_r, the dissipation error of the present scheme is less than the non-compact scheme if $\alpha < 2.1$, and it becomes larger when $\alpha > 2.1$. Table 1 gives the upper limit of the reduced wave number, which corresponds to a point in Fig. 1 where k_r or k_i begins to reach 2% errors relative to their exact solutions, respectively. Larger upper limit of α implies coarse mesh size (Δx) (hence fewer grid points) can be used to resolve a given physical structure. For example, to approximate the exact wave speed within 2% error, the ratio of grid points needed by the upwind compact scheme to those needed by the upwind biased scheme is $0.902/1.61 = 0.56$ in one dimensional case, and it becomes $(0.902/1.61)^2 = 0.31$ in two-dimensional case, resulting in significant saving in grid point numbers. In all, the compact scheme is more efficient than the non-compact scheme when a desired resolution is pursued.

7. Numerical examples

In this section, the present numerical method is tested in one steady flow and three unsteady flow problems. These are the Kovasznay flow, the oscillating plate, the Taylor decaying vortices, and the doubly periodic shear layer. The first three test

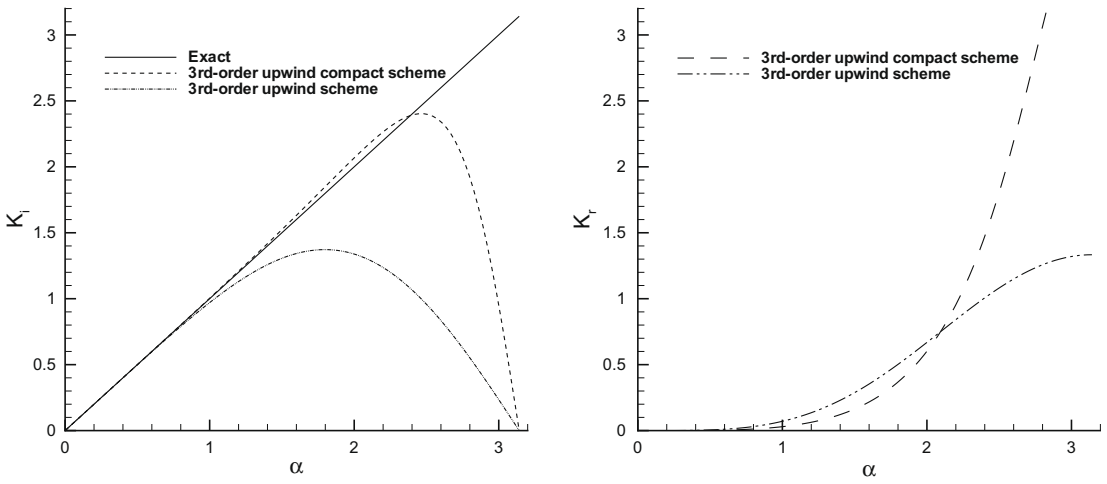

Fig. 1. Variations of k_i and k_r vs. α for the compact and non-compact schemes.

Table 1
Upper limits of the reduced wave number when k_r and k_i of the difference schemes first exceed 2% errors relative to their exact solutions.

Scheme	Upper limits of wave number	
	$k_r < 2\%$	$\lvert 1 - k_i/\alpha \rvert < 2\%$
Upwind compact scheme	0.91	1.61
Upwind biased scheme	0.72	0.902

cases have analytical solutions, while the last one has been studied extensively in the literature. In all these cases, the pseudo-time step $\Delta\tau$ is determined locally with CFL = 10.

7.1. Kovasznay flow

The Kovasznay flow [43] is used for verification of the order of accuracy of the present compact scheme. This problem has an analytical solution to the two-dimensional steady INSE in a square domain $[-0.5 \times 1.5]^2$. The exact solution of the problem is [44]:

$$u = 1 - e^{\lambda x}\cos(2\pi y),$$
$$v = \frac{\lambda}{2\pi}e^{\lambda x}\sin(2\pi y),$$
$$p = p_0 - \frac{1}{2}e^{2\lambda x},$$

where $\lambda = \frac{\mathrm{Re}}{2} - \sqrt{\left(\frac{\mathrm{Re}^2}{4} + 4\pi^2\right)}$, and p_0 is a reference pressure (an arbitrary constant). Drichlet type boundary conditions are specified using the exact solution. We run the unsteady code with a physical-time step $\Delta t = 0.1$ and maximum number of sub-iteration of 100. The calculation is continued until the residual reaches machine zero. The computed streamlines and vorticity contours for $\mathrm{Re} = 40$ are shown in Fig. 2a and b, respectively.

Tables 2 and 3 show grid refinement test results for compact and non-compact schemes, respectively, where the order of accuracy O_A is calculated by the formula

$$O_A = \frac{\ln(e_2/e_1)}{\ln 2.0}$$

with

$$e_1 = |\phi_e - \phi_f|, e_2 = |\phi_e - \phi_c|.$$

ϕ_e, ϕ_f and ϕ_c stands for the exact solution, the solution on a fine grid and the solution on a coarser grid with half of the points in all directions. It clearly demonstrates that the spatial order of accuracy of the present scheme is approximately 3.0 as per our expectation. Looking at the two tables, it is evident that the present compact scheme is a little bit more accurate than the

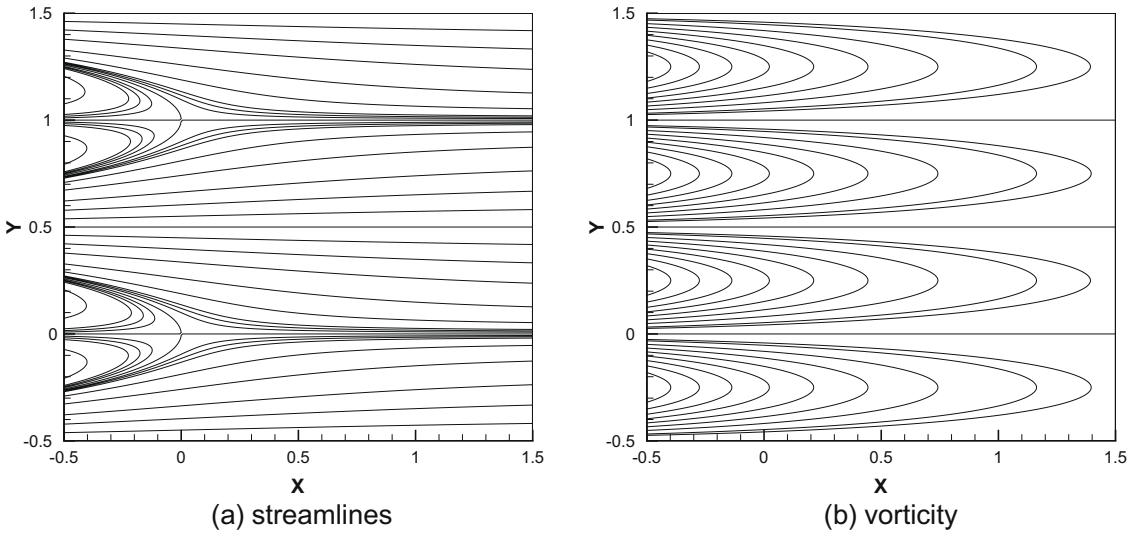

Fig. 2. Streamlines and vorticity contours for the Kovasznay flow at $\mathrm{Re} = 40$.

Table 2
Errors and orders of accuracy using the compact scheme for the Kovasznay flow.

Grid	Re = 1		Re = 20		Re = 40	
	L^2 error	Order	L^2 error	Order	L^2 error	Order
11×11	4.29×10^{-1}	–	6.06×10^{-2}	–	3.26×10^{-2}	–
21×21	7.72×10^{-2}	2.47	1.40×10^{-2}	2.11	7.37×10^{-3}	2.15
41×41	1.38×10^{-2}	2.48	1.73×10^{-3}	3.02	9.48×10^{-4}	2.96
81×81	1.90×10^{-3}	2.86	1.62×10^{-4}	3.42	9.56×10^{-5}	3.31
161×161	2.04×10^{-4}	3.22	1.48×10^{-5}	3.45	9.60×10^{-6}	3.32
321×321	2.48×10^{-5}	3.04	1.40×10^{-6}	3.4	9.59×10^{-7}	3.32
	Re = 100		Re = 500		Re = 1000	
11×11	2.75×10^{-2}	–	1.33×10^{-2}	–	7.94×10^{-3}	–
21×21	3.85×10^{-3}	2.84	2.33×10^{-3}	2.51	1.75×10^{-3}	2.18
41×41	5.06×10^{-4}	2.93	3.08×10^{-4}	2.92	2.35×10^{-4}	2.90
81×81	5.18×10^{-5}	3.29	3.21×10^{-5}	3.26	2.59×10^{-5}	3.18
161×161	5.74×10^{-6}	3.17	3.38×10^{-6}	3.25	2.75×10^{-6}	3.23
321×321	6.64×10^{-7}	3.11	3.94×10^{-7}	3.10	3.17×10^{-7}	3.12

Table 3
Errors and orders of accuracy using the non-compact scheme for the Kovasznay flow.

Grid	Re = 1		Re = 20		Re = 40	
	L^2 error	Order	L^2 error	Order	L^2 error	Order
11×11	5.23×10^{-1}	–	1.25×10^{-1}	–	6.98×10^{-2}	–
21×21	9.14×10^{-2}	2.52	1.65×10^{-2}	2.92	9.72×10^{-3}	2.84
41×41	1.67×10^{-2}	2.45	2.11×10^{-3}	2.97	1.20×10^{-3}	3.02
81×81	2.54×10^{-3}	2.72	2.18×10^{-4}	3.27	1.22×10^{-4}	3.30
161×161	3.47×10^{-4}	2.87	2.43×10^{-5}	3.17	1.34×10^{-5}	3.19
321×321	4.54×10^{-5}	2.93	2.90×10^{-6}	3.07	1.59×10^{-6}	3.07
	Re = 100		Re = 500		Re = 1000	
11×11	5.70×10^{-2}	–	2.99×10^{-2}	–	1.80×10^{-2}	–
21×21	6.99×10^{-3}	3.03	3.88×10^{-3}	2.95	2.31×10^{-3}	2.96
41×41	8.64×10^{-4}	3.02	4.89×10^{-4}	2.99	3.36×10^{-4}	2.78
81×81	9.64×10^{-5}	3.16	6.46×10^{-5}	2.92	5.14×10^{-5}	2.71
161×161	1.17×10^{-5}	3.04	8.19×10^{-6}	2.98	6.72×10^{-6}	2.94
321×321	1.45×10^{-6}	3.01	1.04×10^{-6}	2.98	8.54×10^{-7}	2.98

non-compact scheme in term of accuracy. It is to be noted that results in these tables are obtained with the artificial compressibility factor $\beta = 100$, but they are almost the same as those obtained with $\beta = 1000$. This indicates that the computational accuracy is independent of β.

Fig. 3 shows convergence histories for both compact and non-compact schemes. It is seen that the level of convergence for the compact scheme is a little bit lower than that for the non-compact scheme.

7.2. Oscillating plate

The flow over an infinite oscillating plate is known as Stokes second problem (cf. Ref. [28]). The geometry of the problem is such that the x-axis is set along the plate and the y-axis normal to it. The velocity of the plate is given by

$$u_{\text{plate}} = u_0 \cos(\omega t).$$

The exact solution for this problem is

$$u(y,t) = u_0 \exp(-ky)\cos(\omega t - ky),$$

with $k = \sqrt{\frac{\omega}{2\nu}}$, and ν is the kinematic viscosity. For the present computation, the velocity u_0 was set to unity, the angular frequency ω was set to 2π and the constant k was also set to unity so that $\nu = \pi$. The computational grid had 65×121 grid points distributed uniformly along and normal to the wall direction, respectively. The physical-time step Δt was set to 0.01 and the problem was run over eight cycles after which the transient solution had died and time-periodic response was reached. Fig. 4a shows comparison of the computed velocity profiles with the exact solutions at four different instants

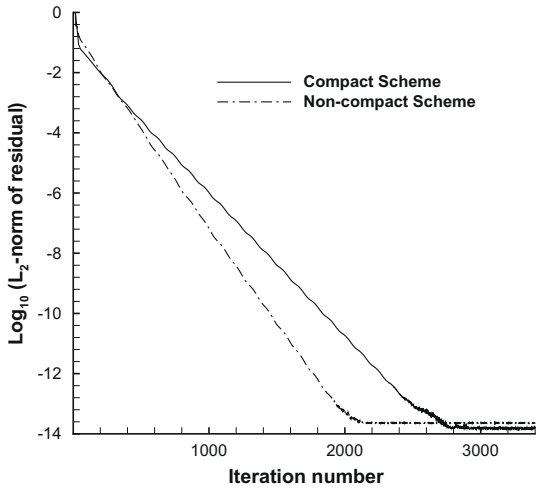

Fig. 3. Convergence histories of compact and non-compact schemes for the Kovasznay flow.

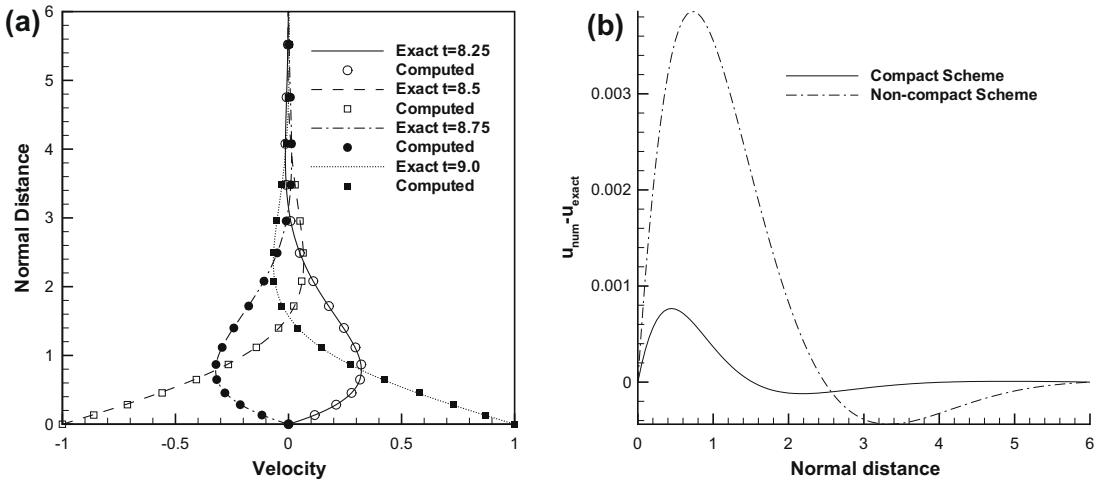

Fig. 4. (a) Computed velocities using the compact scheme and (b) numerical errors for compact and non-compact schemes at $t = 8.25$.

within the 9th cycle. The agreement of the numerical solution with the analytic one is very good. Fig. 4b show the numerical errors for compact and non-compact schemes at $t = 8.25$. It can be seen that the compact scheme produces smaller errors averagely.

7.3. Taylor decaying vortices

The problem of Taylor decaying vortices is frequently used for validation of numerical schemes for simulating unsteady flow problems (cf. Refs. [25,45]). The flow describes an initially periodical vortex structure convected by the flow field and exponentially decaying due to the viscous decaying. The exact solution of the problem satisfying the 2D INSE, is

$$u(x,y,t) = -\cos(x)\sin(y)\exp(-2t/\mathrm{Re})$$
$$v(x,y,t) = \cos(y)\sin(x)\exp(-2t/\mathrm{Re})$$
$$p(x,y,t) = -0.25(\cos 2x + \cos 2y)\exp(-4t/\mathrm{Re})$$

where Re denote the Reynolds number. We present our results computed on a 65×65 uniform grid with $\Delta t = 0.05$, $\beta = 100$ and $\mathrm{Re} = 100$. Fig. 5 shows the computed vorticity contours in domain $[0, 2\pi] \times [0, 2\pi]$ at $t = 2.0$. Fig. 6a and b show comparisons of computed u- and v-velocity components with the exact solution at four different times on the lines passing through the geometric center along the y- and x-axis, respectively. The field-averaged absolute error using the present compact scheme is 2.92×10^{-5}, while that for the non-compact scheme is 7.43×10^{-5}. This implies that the non-compact scheme

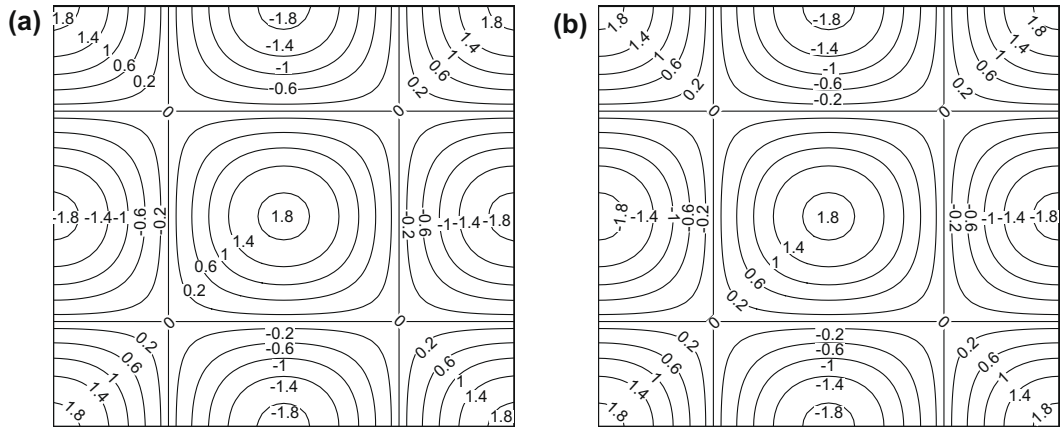

Fig. 5. Vorticity contour for Taylor vortex problem at $t = 2.0$ on a 65×65 grid (a) computed and (b) analytical.

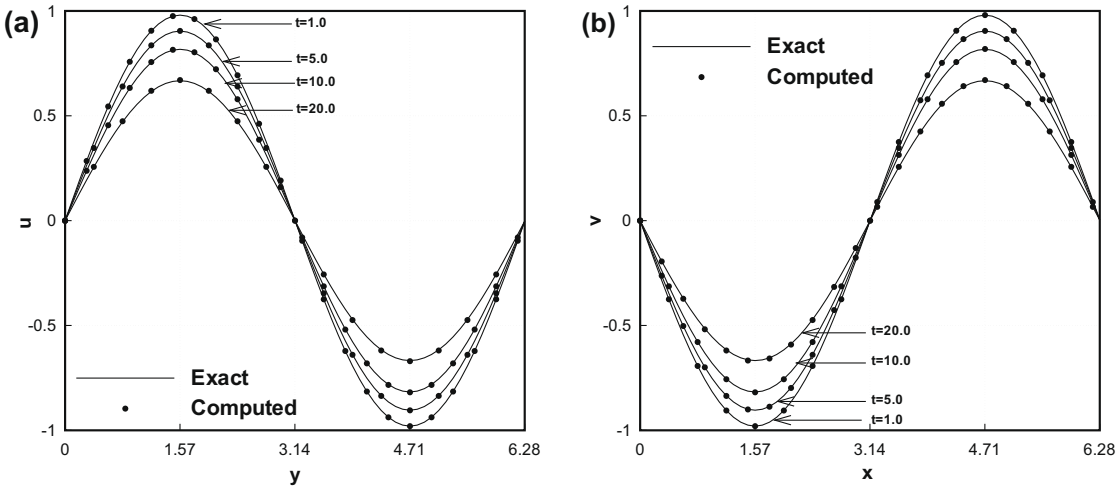

Fig. 6. Comparison of u and v-velocity components along the vertical and horizontal center lines at time levels $t = 1.0$, 5.0, 10.0 and 20.0 for the Taylor vortex problem.

must use much more grid points to obtain the same magnitude of error as the compact scheme. In view of this observation plus the fact that the CPU time of the compact scheme is totally the same as the non-compact scheme, we can say that the compact scheme is superior to the non-compact scheme.

7.4. Doubly periodic shear layer

The flow problem of a doubly periodic pair of shear layers is governed by the INSE in a unit domain $[0,1] \times [0,1]$, subject to the following initial conditions

$$u(x,y,0) = \begin{cases} \tanh[\rho(y-0.25)] \text{ for } y \leqslant 0.5 \\ \tanh[\rho(0.75-y)] \text{ for } y > 0.5 \end{cases},$$
$$v(x,y,0) = v' \sin(2\pi x),$$
$$p(x,y,0) = 0,$$

where ρ determines the thickness of the shear layer (larger ρ corresponds to thinner shear layer), and v' determines the amplitude of the initial perturbation. The correct scenario under the above setup is the perturbed shear layer rolls up into a single vortex as the flow evolves [47]. This is a benchmark problem for testing the accuracy and the resolution of a time-dependent numerical scheme. It was introduced by Bell and Colella [46] and examined later by Minon [47] using a number of schemes to reveal the effects of grid resolution. Di et al. [48] used their moving mesh method to enhance the resolution and

suppress the spurious vortices. These studies have concluded that under-resolution (in scheme accuracy or mesh size) can produce non-physical spurious vortices, and grid resolution has substantial effect on the vorticity field.

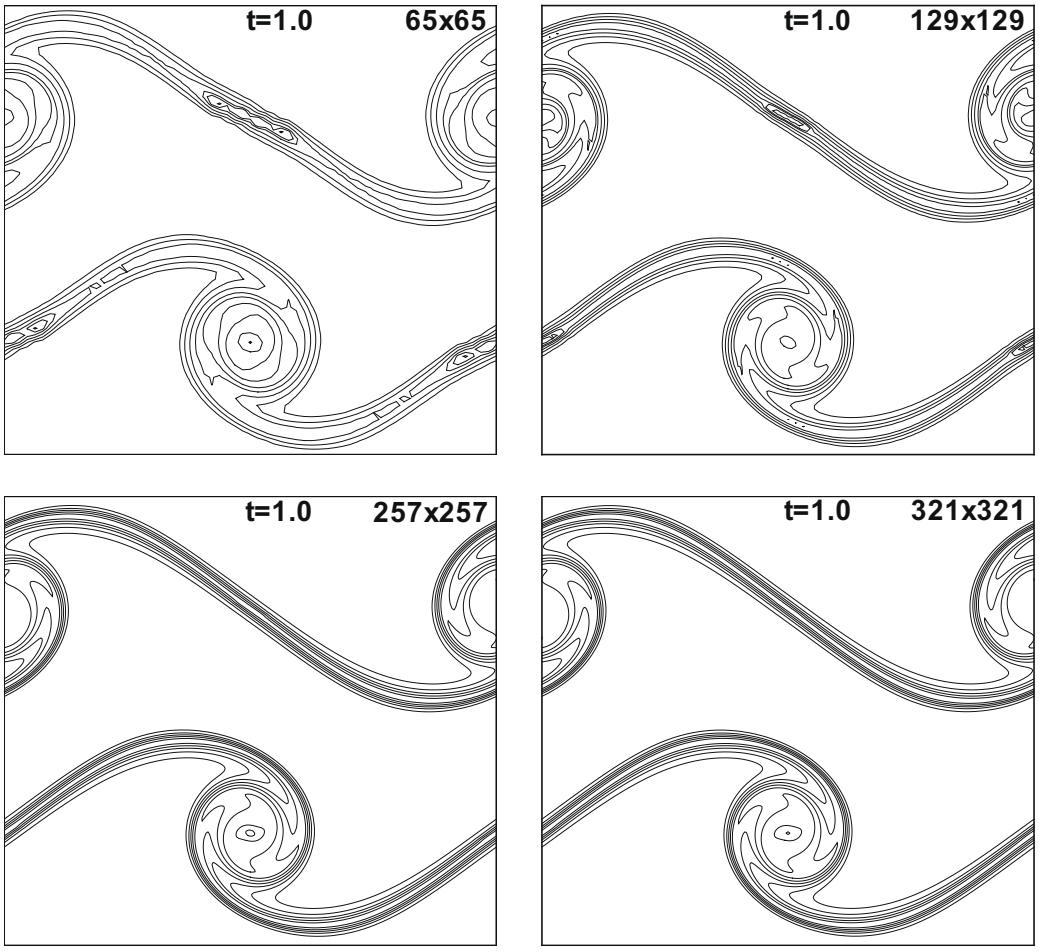

Fig. 7. Vorticity contours for the doubly periodic shear layer problem at $t = 1.0$ obtained on $65 \times 65, 129 \times 129, 257 \times 257$, and 321×321 grids, respectively. Spurious vortices occur on the former two grids.

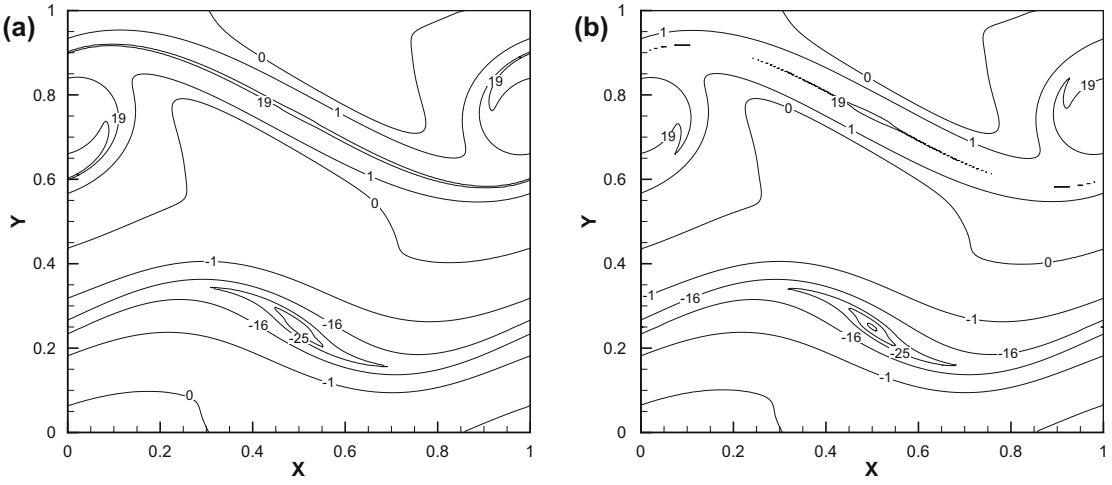

Fig. 8. Vorticity contours at $t = 1$ on grid 257×257 (a) compact scheme and (b) non-compact scheme.

In our computation, the perturbation amplitude was $v' = 0.05$, the thickness parameter was $\rho = 30$, and the Reynolds number was $\mathrm{Re} = 10,000$. Vorticity contours obtained using four different grid resolutions are shown in Fig. 7 for a time $t = 1$. The results obtained with 65×65 and 129×129 grids have small spurious vortices middle way between two big rolled vortices, while those obtained with 257×257 and 321×321 grids do not have. The results obtained with 257×257 grid are qualitatively comparable with the results on 513×513 mesh with a third-order non-compact scheme given in [47]. Actually, the grid independent result is nearly obtained on 257×257 grid, evidenced from the vorticity distribution along a vertical line $x = 0.5$.

Fig. 8 shows comparison between the present compact scheme and its non-compact version on the 257×257 grid for time $t = 1$. It can be seen that the compact scheme produces smooth contour lines for the value $\omega = 19$, but the non-compact scheme has a small closed contour line for the same vorticity value, which is the trace of a spurious eddy just as shown for the case of 129×129 in Fig. 7. This again shows that the compact scheme is better than the non-compact scheme.

8. Conclusions

We have implemented a third-order accurate upwind compact finite difference scheme for time-accurate numerical solution of the incompressible Navier–Stokes equations via dual-time stepping technique. The method is based on the artificial compressibility approach and the flux-difference splitting method. The upwind compact scheme is used to discretize the convective terms while the viscous terms are approximated with a fourth-order central compact scheme. Formulas for the compact schemes, their boundary schemes, and their implementation with the Beam-Warming approximate factorization, are presented in detail. The upwind compact scheme is tested for 2D benchmark flow problems with low to moderate Reynolds numbers and compared with the non-compact scheme in terms of accuracy and CPU time. Comparisons demonstrate that the third-order upwind compact scheme has the same computational cost as the non-compact scheme, but is more accurate.

Acknowledgments

The work of A. Shah was financially supported by CIIT (IDB-1306) and L. Yuan was supported by Natural Science Foundation of China (G10531080 and G10729101) and State Key Program for Developing Basic Sciences (2005CB321703). We would like to thanks the referees for their comments and suggestions and Prof. Michele Napolitano, Department of Mechanical and Industrial Engineering, University of Bari, Italy for providing his FORTRAN subroutine [42].

References

[1] P.M. Gresho, Incompressible fluid dynamics: some fundamental formulation issues, Ann. Rev. Fluid Mech. 23 (1991) 413–453.
[2] P. Orlandi, Fluid Flow Phenomena: A Numerical Toolkit, Kluwer Academic Publishers, 1999.
[3] R. Peyret, Spectral Methods for Incompressible Viscous Flow, Springer, New York, 2001.
[4] C. Canuto, M.Y. Hussaini, A. Quarteroni, T.A. Zhang, Spectral Methods in Fluid Dynamics, Springer, New York, 1988.
[5] R.S. Hirsh, High-order accurate difference solutions of fluid mechanics problems by a compact differencing technique, J. Comput. Phys. 19 (1975) 90–109.
[6] S.G. Rubin, P.K. Khosla, Polynomial interpolation methods for viscous flow calculations, J. Comput. Phys. 24 (1977) 217–244.
[7] S.K. Lele, Compact finite difference schemes with spectral-like resolution, J. Comput. Phys. 103 (1992) 16–42.
[8] W. E, J.-G. Liu, Essentially compact schemes for unsteady viscous incompressible flows, J. Comput. Phys. 126 (1996) 122–138.
[9] M. Li, T. Tang, B. Fornberg, A compact fourth-order finite difference scheme for the steady incompressible Navier–Stokes equations, Int. J. Numer. Meth. Fluids 20 (1995) 1137–1151.
[10] H.L. Meitz, H.F. Fasel, A compact difference scheme for the Navier–Stokes equations in velocity–vorticity formulation, J. Comput. Phys. 157 (2000) 371.
[11] A. Brüger, B. Gustafsson, P. Lötstedt, J. Nilsson, High-order accurate solution of the incompressible Navier–Stokes equations, J. Comput. Phys. 203 (2005) 49.
[12] R.K. Shukla, M. Tatineni, X. Zhong, Very high-order compact finite difference schemes on non-uniform grids for incompressible Navier–Stokes equations, J. Comput. Phys. 224 (2007) 1064–1094.
[13] N.A. Adams, K. Shariff, A high-resolution hybrid compact-ENO scheme for shock–turbulence interaction problems, J. Comput. Phys. 127 (1996) 27.
[14] D.X. Fu, Y.W. Ma, High resolution scheme, in: M. Hafez, K. Oshima (Eds.), Computational Fluid Dynamics Review, Wiley, 1995, pp. 234–250.
[15] D.X. Fu, Y.W. Ma, T. Kobayashi, Non-physical oscillations in numerical solutions: reason and improvement, CFD J. 4 (4) (1996) 427–450.
[16] D.X. Fu, Y.W. Ma, A high-order accurate finite difference scheme for complex flow fields, J. Comput. Phys. 134 (1997) 1–15.
[17] X. Deng, H. Maekawa, Compact high-order accurate nonlinear schemes, J. Comput. Phys. 130 (1997) 77.
[18] S. Pirozzoli, Conservative hybrid compact-WENO schemes for shock–turbulence interaction, J. Comput. Phys. 178 (2002) 81–117.
[19] Y.Q. Shen, G.W. Yang, Z. Gao, High-resolution finite compact differences for hyperbolic conservation laws, J. Comput. Phys. 216 (2006) 114–137.
[20] D.V. Gaitonde, J.S. Shang, J.L. Young, Practical aspects of higher-order numerical schemes for wave propagation phenomena, Int. J. Numer. Meth. Engrg. 45 (1999) 1849–1869.
[21] J.P. Boyd, Chebyshev and Fourier Spectral Methods, second ed., Dover, Mineola, USA, 2000.
[22] A.I. Tlstykh, M.V. Lipavskii, On performance of methods with third and fifth-order compact upwind differencing, J. Comput. Phys. 140 (1998) 205–232.
[23] F.H. Harlow, L.F. Welch, Numerical calculation of time-dependent viscous incompressible flow of fluid with free surface, Phys. Fluids 8 (1965) 2182–2189.
[24] A.J. Chorin, Numerical solution of the Navier–Stokes equations, Math. Comput. 22 (1968) 742–762.
[25] J. Kim, P. Moin, Application of a fractional step methods to incompressible Navier–Stokes equations, J. Comput. Phys. 59 (1985) 308–323.
[26] S.V. Patankar, D.B. Spalding, A calculation procedure for heat, mass and momentum transfer in three-dimensional parabolic flows, Int. J. Heat Mass Transfer 15 (1972) 1787–1806.
[27] A.J. Chorin, A numerical method for solving incompressible viscous flow problems, J. Comput. Phys. 2 (1967) 12–26.
[28] S.E. Rogers, D. Kwak, An upwind differencing scheme for the time-accurate incompressible Navier–Stokes equations, AIAA J. 28 (2) (1990) 253–262.
[29] S.E. Rogers, D. Kwak, An upwind differencing scheme for the incompressible Navier–Stokes equations, Appl. Numer. Math. 1 (8) (1991) 43–64.

[30] D. Choi, C.L. Merkle, Application of time-iterative schemes to incompressible flow, AIAA J. 23 (1985) 1518–1524.
[31] C.L. Mercle, M. Athavale, Time-accurate unsteady incompressible flow algorithm based on artificial compressibility method, AIAA Paper 87-1137, AIAA Press Washington DC, 1987.
[32] Li Yuan, Comparison of implicit multigrid schemes for three-dimensional incompressible flows, J. Comput. Phys. 177 (2002) 134–155.
[33] P.M. Hartwich, C.H. Hsu, An implicit flux-difference splitting scheme for 3D incompressible N–S solutions to leading edge vortex flow, AIAA Paper 86-1839, 1986.
[34] W. Briley, S. Neerarambam, D. Whitfield, Implicit lower–upper approximate factorization schemes for incompressible flows, J. Comput. Phys. 128 (1996) 32–42.
[35] J.Y. Yang, S.C. Yang, Y.N. Chen, C.A. Hsu, Implicit weighted ENO schemes for three-dimensional incompressible Navier–Stokes equations, J. Comput. Phys. 146 (1998) 464–487.
[36] J. Ekarterinaris, High-order accurate numerical solutions of incompressible flows with the artificial compressibility method, Int. J. Numer. Meth. Fluids 45 (2004) 1187–1207.
[37] Abdullah Shah, Hong Guo, Li Yuan, A third-order upwind compact scheme on curvilinear meshes for the incompressible Navier–Stokes equations, Commun. Comput. Phys. 5 (2–4) (2009) 712–729.
[38] A.K. De, V. Eswaran, Analysis of a new high resolution upwind compact scheme, J. Comput. Phys. 218 (2006) 398–416.
[39] P.L. Roe, Approximate Riemann solvers, parameter vectors, and difference scheme, J. Comput. Phys. 43 (1981) 357–372.
[40] R. Beam, R.F. Warming, An implicit scheme for the compressible Navier–Stokes equations, AIAA J. 16 (1978) 393–402.
[41] T.H. Pulliam, D.S. Chaussee, A diagonalized form of an implicit approximate factorization algorithm, J. Comput. Phys. 39 (2) (1981) 347–363.
[42] M. Napolitano, A FORTRAN subroutine for the solution of periodic block-tridiagonal systems, Commun. Appl. Numer. Meth. 1 (1985) 11–15.
[43] L.S.G. Kovasznay, Laminar flow behind a two-dimensional grid, Proc. Camb. Philos. 44 (1948) 58.
[44] V. Prabhakar, J.N. Reddy, Spectral/hp penalty least-square finite element formulation for the steady incompressible Navier–Stokes equations, J. Comput. Phys. 215 (2006) 274–297.
[45] A. Quarteroni, F. Saleri, A. Veneziani, Factorization methods for the numerical approximation of Navier–Stokes equations, Comput. Meth. Appl. Mech. Engrg. 188 (2000) 505–526.
[46] J.B. Bell, P. Colella, H. M Glaz, An efficient second-order projection method for the incompressible Navier–Stokes equations, J. Comput. Phys. 85 (1989) 257–283.
[47] M.L. Minon, D. Brown, Performance of under-resolved two-dimensional incompressible flow simulation: II, J. Comput. Phys. 138 (1997) 734–765.
[48] Yana Di, Rou Li, Tao Tang, Pinggwin Zhang, Moving mesh finite element methods for the incompressible Navier–Stokes equations, SIAM J. Sci. Comput. 26 (2005) 1036–1056.